Mechanical Systems and Signal Processing 91 (2017) 81–92

Contents lists available at ScienceDirect

Mechanical Systems and Signal Processing

journal homepage: www.elsevier.com/locate/ymssp

Using instability to reconfigure smart structures in a spring-mass model

Jiaying Zhang [a,b,*], Colin R. McInnes [b]

[a] Department of Mechanical and Aerospace Engineering, University of Strathclyde, Glasgow G1 1XJ, United Kingdom
[b] School of Engineering, University of Glasgow, Glasgow G12 8QQ, United Kingdom

ARTICLE INFO

Article history:
Received 14 June 2016
Received in revised form 14 October 2016
Accepted 25 November 2016
Available online 10 January 2017

Keywords:
Multistable
Reconfiguration
Energy-efficient
Heteroclinic connections
Dissipation

ABSTRACT

Multistable phenomenon have long been used in mechanism design. In this paper a subset of unstable configurations of a smart structure model will be used to develop energy-efficient schemes to reconfigure the structure. This new concept for reconfiguration uses heteroclinic connections to transition the structure between different unstable equal-energy states. In an ideal structure model zero net energy input is required for the reconfiguration, compared to transitions between stable equilibria across a potential barrier. A simple smart structure model is firstly used to identify sets of equal-energy unstable configurations using dynamical systems theory. Dissipation is then added to be more representative of a practical structure. A range of strategies are then used to reconfigure the smart structure using heteroclinic connections with different approaches to handle dissipation.

1. Introduction

Many structures are designed to be multi-stable equilibrium systems, so-called compliant mechanisms such as bi-stable mechanism and tri-stable mechanisms. These mechanisms store energy in some initial position and then release the stored energy through motion to another stable position [1]. For example, a discrete truss model, which consists of two bars connected by pin joints, has been investigated as a pseudo-bistable structure for morphing [2]. Others have investigated a thin-walled bi-stable geometry from natural systems and origami design principles. Finite element analysis and experimental results show the bi-stability of a reinforced silicone elastomer [3]. However, unstable equilibria could be considered to connect different configurations, as presented by Guenther et al. [4]. Some special anisotropic patterning of structures can help deal with instability [5]. Moreover, active control can be used to maintain the structure in an unstable state using an agent-based approach, which controls the structure to suppress instability [6]. Such active control can in principle allow the use of heteroclinic connections to transition a smart structure between unstable states.

A large number of engineering application have been investigated using multi-stable devices, for example an advanced helicopter rotor blade has used them for morphing to generate additional lift-load [7]. An adaptive antennae has been designed by synthesising compliant mechanisms to enable a morphing approach from a given curve into a target curve [8]. In addition, some simple models have analysed the stability of a buckled elastic beam, using an applied a load as an actuator for snap-through phenomenon [9], while experiment results show the detailed dynamics of the buckled beam as

* Corresponding author at: Department of Mechanical and Aerospace Engineering, University of Strathclyde, Glasgow G1 1XJ, United Kingdom.
E-mail address: jiaying.zhang@strath.ac.uk (J. Zhang).

http://dx.doi.org/10.1016/j.ymssp.2016.11.029
0888-3270/

compared to numerical results [10]. Meanwhile, the properties of lightweight components in mechatronic devices can produce quick and precise movement or forces. A range of such components are designed and manufactured using smart materials, whose properties are controlled by external stimuli such as moisture, temperature, electric or magnetic fields [11,12]. There are a number of types of smart materials with various characteristics, such as shape memory alloys (SMAs), temperature-responsive polymers (TMPs) and piezoelectric materials. Currently, a wide range of SMA actuators have been successfully applied in low frequency vibration and actuation applications [13]. Furthermore, recent research shows that structures made of shape-memory polymers can provide large deformation under active control [14,15]. Broad applications of such smart materials can be found in the Aerospace, Energy and Marine sectors, particularly for energy harvesting, vibration control and structural health monitoring [16]. In addition, several unconventional applications have arisen, for example a self-folding origami structure was presented, constructed using shape memory composites that could be activated with uniform heating [17]. Moreover, a crawling robot has also been investigated which can fold itself from a flat sheet with embedded electronics, such as shape-memory composites, and can transform itself into a functional machine [18]. A single sheet can be reconfigured to desired shapes through multiple controllers by an optimised design [19].

In previous work, a simple model of a smart structure was presented by McInnes and Waters [20]. The model comprised a two mass chain with three springs which were approximated to provide simple cubic nonlinearity. Then, dynamical system theory was used to investigate the characteristics of this simplified system to identify both stable and unstable equilibrium configurations, some of which were connected using heteroclinic connections. This cubic nonlinear model has also been used to investigate vibrational energy harvesting through the use of stochastic resonance [21]. The cubic model is considered as a simple mechanical system which can change its kinematic configuration between a finite set of stable or unstable equilibria. The equal energy unstable equilibria are connected through heteroclinic paths in the phase space of the problem. Therefore, in principle zero net energy is required to achieve transitions between these configurations in the absence of dissipation. Numerical results illustrated that reconfiguration between unstable equilibria can in principle be energetically efficient compared to transitions between stable configurations, which need to cross a potential barrier. In addition, a reconfiguration method based on a reference trajectory and an inverse control method has been applied to this cubic model and then extended to a more complex model for which it is difficult to generate heteroclinic connections numerically. It is envisaged that being computationally efficient, the strategy could form the basis of real-time reconfiguration of smart structures. [22].

In this paper a more complex and realistic spring-mass model is developed to consider the differences between the cubic approximation used in previous work and a real spring model with dissipation, which illustrates the possibility of using heteroclinic connections to reconfigure real smart structures, expanding on Ref. [23]. Again, a set of equilibria can be found and can in principle be connected through heteroclinic paths. Then, strategies are considered to deal with the dissipation term. Two control methods are investigated, using an end-point control and an optimal control strategy. In addition, a bifurcation control strategy is investigated which allows the stability properties of the equilibria to be controlled, enabling stable equilibria to become temporarily unstable and so connected by heteroclinic paths. Numerical results are presented to illustrate the control strategies developed.

2. Smart structure model

Consider a simply clamped smart structure model, which consists of a two mass chain connected by three linear springs of stiffness (k_1, k_2, k_3) and natural lengths (L_1, L_2, L_3), as illustrated in Fig. 1. It is assumed that the masses can only move in the vertical direction. If the displacement of a mass is defined by $\boldsymbol{x}(x_1, x_2)$, while the spring clamps are separated by $3d$, it can be shown that the spring lengths after deformation are described by

$$l_1 = \sqrt{(x_1^2 + d^2)} \tag{1}$$

$$l_2 = \sqrt{((x_1 - x_2)^2 + d^2)} \tag{2}$$

$$l_3 = \sqrt{(x_2^2 + d^2)} \tag{3}$$

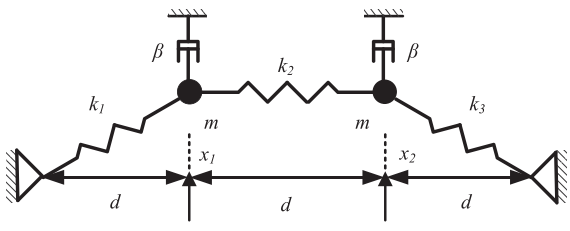

Fig. 1. 2 degree-of-freedom bucking beam model with damping coefficient β.

In order to investigate the characteristics of the system, it is assumed that the structure can initially be considered as a Hamiltonian system (without dissipation) with a simplification of unit mass m. From Fig. 1, the Hamiltonian for this system can then be defined from the kinetic and potential energy with spring natural length $\boldsymbol{L}(L_1, L_2, L_3)$ through Eqs. (4) and (5)

$$T(\boldsymbol{p}) = \frac{1}{2}(p_1^2) + \frac{1}{2}(p_2^2) \tag{4}$$

$$V(\boldsymbol{x}, \boldsymbol{L}) = \frac{1}{2}k_1(l_1 - L_1)^2 + \frac{1}{2}k_2(l_2 - L_2)^2 + \frac{1}{2}k_3(l_3 - L_3)^2 \tag{5}$$

with momentum coordinates $\boldsymbol{p}(p_1, p_2)$ associated with position coordinates $\boldsymbol{x}(x_1, x_2)$.

However, for a realistic model dissipation must also be considered, which of course will destroy the Hamiltonian structure of the dynamics. Therefore, phase trajectories from one unstable equilibrium point cannot reach another equal-energy unstable equilibrium point. In order to compensate for such dissipation, controllers need to be used to ensure that heteroclinic connections exist. Therefore, the dynamics of the problem can be extended by the addition of linear dissipation parameterised by β, as shown in Fig. 1.

The problem can now fully defined by a dynamical system of the form

$$\dot{x_1} = p_1 \tag{6}$$

$$\dot{p_1} = \frac{(L_1 - \sqrt{(x_1^2 + 1)})k_1 x_1}{\sqrt{(x_1^2 + 1)}} + \frac{(L_2 - \sqrt{((x_1 - x_2)^2 + 1)})k_2(x_1 - x_2)}{(\sqrt{(x_1 - x_2)^2 + 1})} - \beta p_1 \tag{7}$$

$$\dot{x_2} = p_2 \tag{8}$$

$$\dot{p_2} = \frac{(L_3 - \sqrt{(x_2^2 + 1)})k_3 x_2}{\sqrt{(x_2^2 + 1)}} - \frac{(L_2 - \sqrt{((x_1 - x_2)^2 + 1)})k_2(x_1 - x_2)}{(\sqrt{(x_1 - x_2)^2 + 1})} - \beta p_2 \tag{9}$$

Then, using dynamical system theory to analyse the system defined by Eqs. (6)–(9), it can be shown that there exists a number of both stable and unstable equilibria which may be connected in phase space. One such type of path is the heteroclinic connection, which requires that the stable and unstable manifolds of two equal-energy unstable equilibria are connected. Solving Eqs. (6)–(9) for equilibrium solutions yields 13 equilibria for the parameter set, $k_1 = k_2 = k_3 = 1$, $d = 1$, $L_1 = L_2 = L_3 = 2.5$. The details of the equilibria are listed in Table 1.

Moreover, the stability properties of these equilibria can be determined from the Hessian matrix of the potential energy. In the second derivative test for determining extrema of the potential function $V(\boldsymbol{x}, \boldsymbol{L})$, the discriminant D is given by

$$D = \begin{vmatrix} \frac{\partial^2 V}{\partial x_1^2} & \frac{\partial^2 V}{\partial x_1 \partial x_2} \\ \frac{\partial^2 V}{\partial x_2 \partial x_1} & \frac{\partial^2 V}{\partial x_2^2} \end{vmatrix} \tag{10}$$

Through using the second derivative test discriminant [23], it can be shown that the system possesses 1 unstable equilibrium E_0 with a global potential maximum, 6 stable equilibria E_1 to E_6 with a global potential minimum and 6 unstable equilibria E_7 to E_{12} where the potential has a saddle, as can be seen in Fig. 2. The corresponding shapes of the structure are shown in Fig. 3, which presents different configurations associated with each of the 13 equilibria. Meanwhile, it can be seen from Table 1 and Fig. 2 that E_0 has the highest potential V with each spring in compression while E_7 to E_{12} are unstable equilibria which have only one spring in compression and the stable equilibria E_1 to E_6 have both springs extended.

Table 1
Stability properties of the 13 equilibria of 2 degree-of-freedom bucking beam model.

Point	$\tilde{x}_1$	$\tilde{x}_2$	V(potential)	D	Type
E_0	0	0	3.38	1.75	Maximum
E_1	1.48	−1.48	0.70	1.35	Minimum
E_2	−1.48	−2.96	0.70	1.35	Minimum
E_3	−2.96	−1.48	0.70	1.35	Minimum
E_4	−1.48	1.48	0.70	1.35	Minimum
E_5	1.48	2.96	0.70	1.35	Minimum
E_6	2.96	1.48	0.70	1.35	Minimum
E_7	0	2.29	1.13	−1.81	Saddle
E_8	2.29	2.29	1.13	−1.81	Saddle
E_9	2.29	0	1.13	−1.81	Saddle
E_{10}	0	−2.29	1.13	−1.81	Saddle
E_{11}	−2.29	−2.29	1.13	−1.81	Saddle
E_{12}	−2.29	0	1.13	−1.81	Saddle

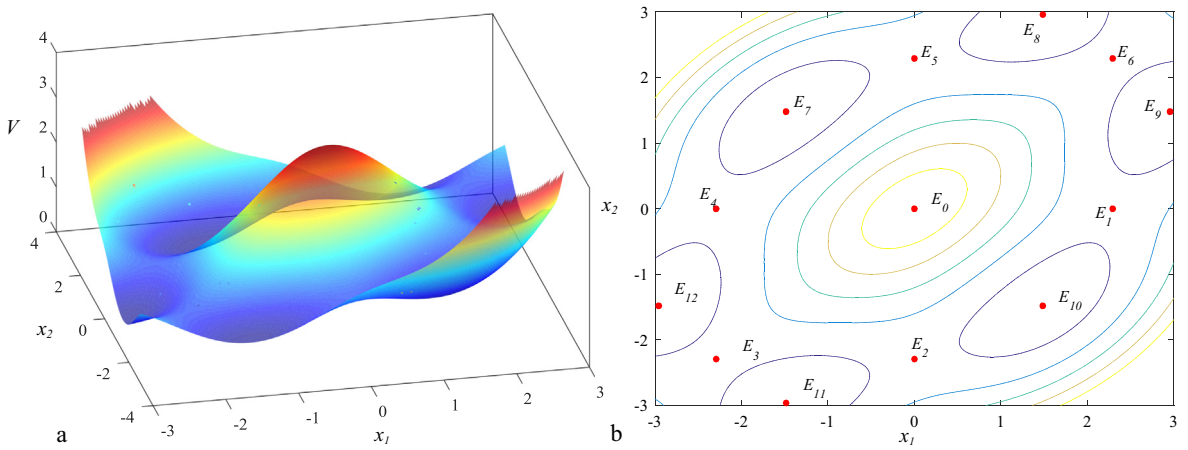

Fig. 2. Potential $V(\boldsymbol{x},\boldsymbol{L})$ and equilibria (6 stable equilibria E_1 to E_6, and 6 unstable equilibria E_7 to E_{12}). (a) 3D surface plot. (b) Contour plot.

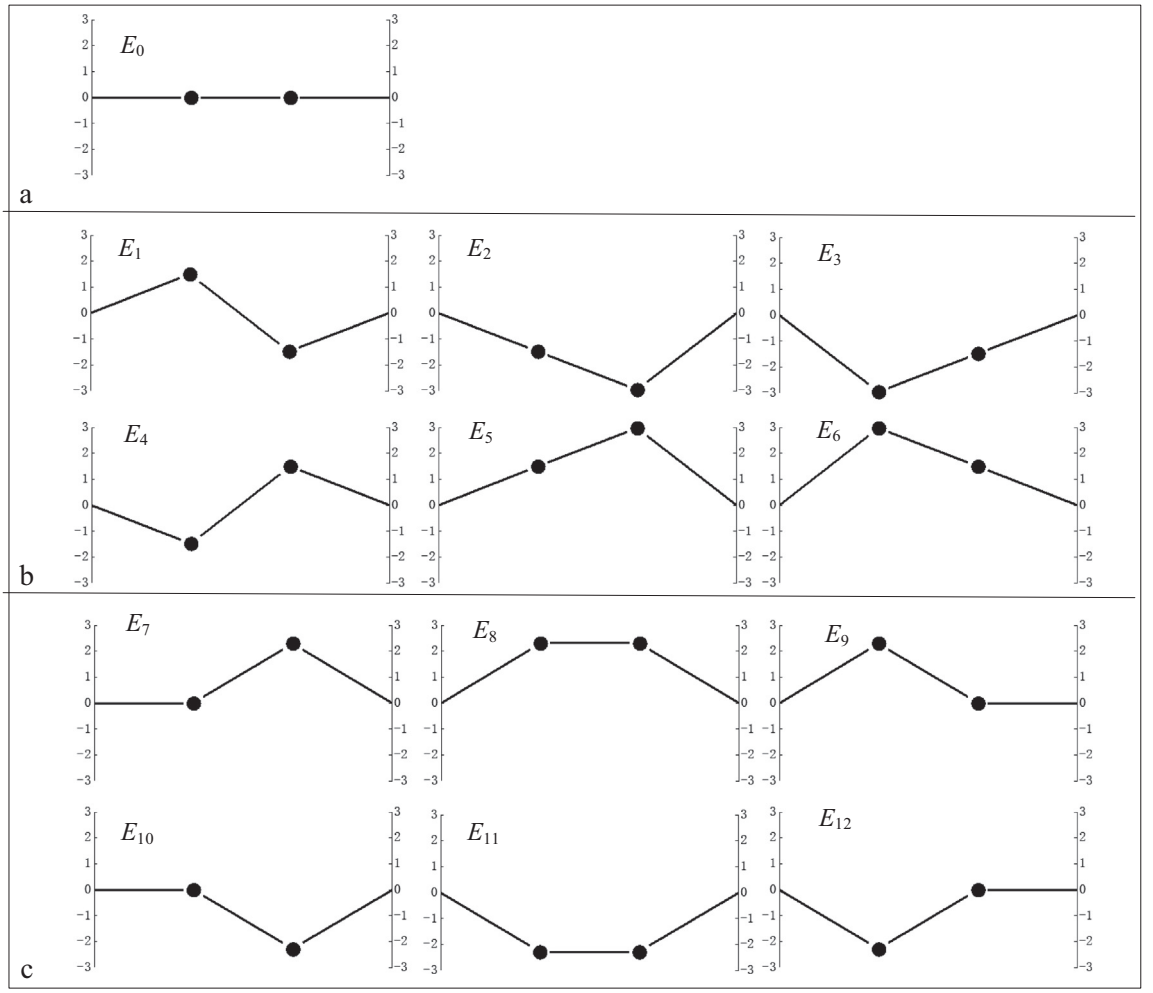

Fig. 3. Equilibria for a two mass chain with (a) maximum potential equilbria E_0 (b) stable equilbria $E_{1\text{-}6}$ and (c) unstable equilibria $E_{7\text{-}12}$.The unstable equilibria have equal potential V.

Using dynamical system theory, we can then generate the stable and unstable manifolds of the unstable equilibria to seek possible connections between them [24]. For the conservative system, linearisation of Hamilton's equations in the neighbourhood of each equilibrium point yields pairs of positive and negative eigenvalues with the corresponding eigenvectors for the stable and unstable direction $\boldsymbol{u}^s$ and $\boldsymbol{u}^u$ associated with each eigenvalue. These eigenvectors $\boldsymbol{u}^s$ and $\boldsymbol{u}^u$ are tangent to the stable manifold $\boldsymbol{W}_s$ and the unstable manifold $\boldsymbol{W}_u$ in the neighbourhood of each equilibrium [20]. Therefore, the eigenvectors can be mapped to approximate the stable and unstable manifolds by integrating forwards or backwards from an unstable equilibrium point $\boldsymbol{t}^e$, defined by

$$\boldsymbol{t}^s = \boldsymbol{t}^e + \epsilon \boldsymbol{u}^s \tag{11}$$

$$\boldsymbol{t}^u = \boldsymbol{t}^e + \epsilon \boldsymbol{u}^u \tag{12}$$

for $\epsilon \ll 1$ $\boldsymbol{t} = (\boldsymbol{x}, \boldsymbol{p}) \in \mathbf{R}^4$. While this method can be used to find heteroclinic connections between equal-energy unstable equilibria, a means to stabilise the structure before and after such a reconfiguration must firstly be sought.

3. Bifurcation control

In previous work [23], a numerical search technique for reconfiguration using heteroclinic connections without dissipation was investigated. It was assumed that the instability of the equal-energy unstable equilibria could be compensated by using active control. However, an alternative bifurcation control method may be considered if the natural length of the springs L_{1-3} can be manipulated, for example if the springs are manufactured from an appropriate shape memory alloy. A conservative Hamiltonian system is assumed initially, with compensation for dissipation considered later in Section 4.

A 'ball on a hill' model can be used to provide a schematic illustration of the proposed bifurcation control method, as shown in Fig. 4. The potential energy of the ball depends on its position on the hill so that a heteroclinic can connection exist between two hills (Fig. 4b). Fig. 4a shows the ball on the first hill, which is initially locally stable. Then through manipulating the local shape of the first hill it becomes unstable to effect the heteroclinic connection to the second hill, which can subsequently transition from unstable to locally stable, as shown in Fig. 4b and c.

Based on this simple illustrative model, a new reconfigurable strategy is investigated using the spring-mass smart structure model detailed in Section 2.

In order to illustrate this strategy directly, L_2 is firstly manipulated and changed from 1 to 2.5 with L_1 and L_3 fixed. Initially a large change in the spring natural length is considered for clarity of illustration; a smaller change will be used later. It can be seen from Fig. 5 that the number of equilibria will change with an increase of L_2, which is shown by the equilibria $\tilde{x}_1$ at different lengths of L_2. Moreover, there are three invariant points (0,0), $(\sqrt{3}, \sqrt{3})$ and $(-\sqrt{3}, -\sqrt{3})$ whose locations are independent of L_2. For $L_2 = 1$ the equilibria E_1 and E_2 are stable, and the potential forms local minima at these locations, as shown in Fig. 6. Then, if L_2 is increased such that $L_2 \geqslant 2$, the equilibria $(\sqrt{3}, \sqrt{3})$ and $(-\sqrt{3}, -\sqrt{3})$ became unstable and a heteroclinic connection can be used to reconfigure the structure between these two equilibria, as shown in Fig. 7. After the reconfiguration, L_2 is finally decreased such that $L_2 = 1$ and the system becomes stable again. This scheme allows operation of the structure in a stable state, a transition to instability to reconfigure the structure, and then continued operation in another stable state.

A transition using this scheme (without dissipation) is shown in Fig. 8. The coupling parameters are $L_1 = 2$ and $L_3 = 2$ with L_2 switched from 2.5 to 1 to manipulate the stability properties of E_1 and E_2. Firstly, a small displacement is added to the system in the local minimum potential well to demonstrate capture at the equilibrium point. This initial oscillation of the system in the potential well at E_1 with $L_2 = 1$ can be seen, followed by a transition to E_2 with $L_2 = 2.5$ after the bifurcation and then a return to oscillation in the local minimum potential well at E_2 with $L_2 = 1$.

In order to further explore the possibility of reconfiguring the smart structure using bifurcation control, a more complex situation will now be considered. Figs. 2 and 5 show that the equilibria $(\sqrt{3}, \sqrt{3})$ and $(-\sqrt{3}, -\sqrt{3})$ became unstable when $L_2 = 2$, but with the same potential energy as other saddle points such as $(0, \sqrt{3})$. An iterative approach [25], can also be used which divides a position coordinate, such as x_1, into several steps with a desired increment, then the other position coordinate x_2 can be used to seek to minimise the potential energy of every step. Therefore, an ideal path can be generated on the potential energy contour from $(\sqrt{3}, \sqrt{3})$ to $(-\sqrt{3}, -\sqrt{3})$ with $L_1 = L_2 = L_3 = 2$. This results in a series of connected hetero-

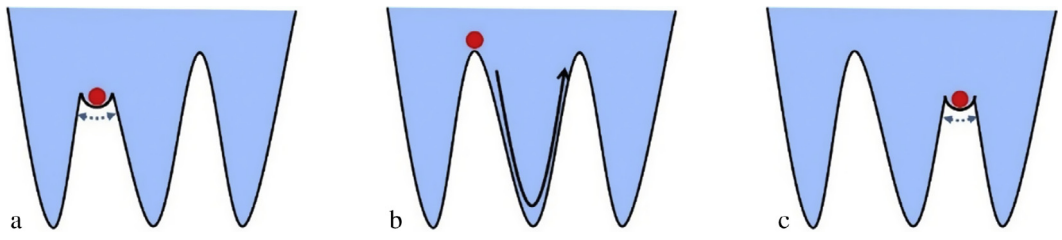

Fig. 4. Schematic representation of bifurcation control (a) and (c) are different locally stable configurations of the structure (b) heteroclinic connection between the two equal-energy unstable configurations.

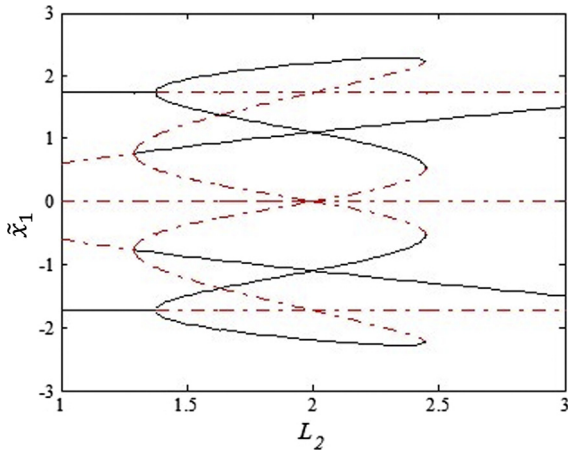

Fig. 5. Bifurcation diagram for the spring-mass model. Projection of the location of the equilibria onto the x_1 axis for $L_1 = 2$, $L_3 = 2$ and $1 \leqslant L_2 \leqslant 3$. Solid line: stable equilibria, dashed line: unstable equilibria.

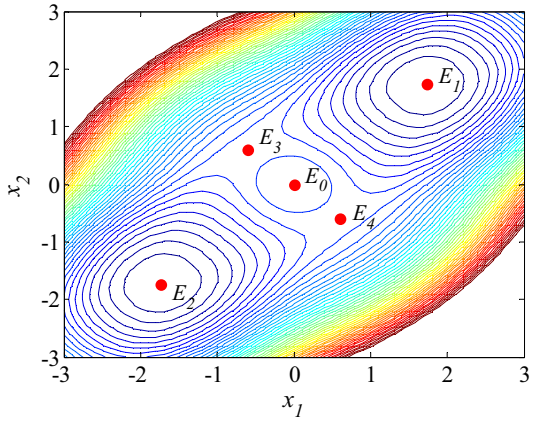

Fig. 6. Effective potential $V(\boldsymbol{x}, \boldsymbol{L})$ with $L_1 = 2$, $L_2 = 1$ and $L_3 = 2$. E_1 and E_2 are stable, E_3 and E_4 are unstable.

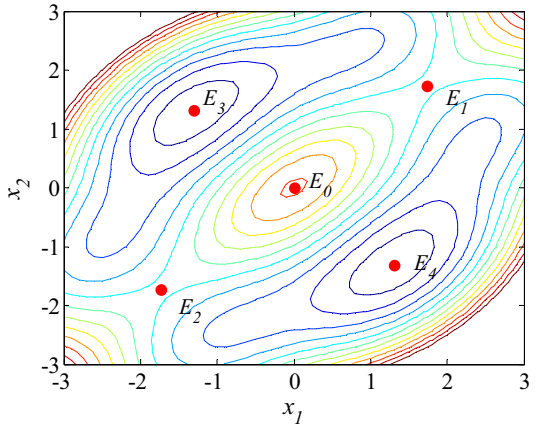

Fig. 7. Effective potential $V(\boldsymbol{x}, \boldsymbol{L})$ with $L_1 = 2$, $L_2 = 2.5$ and $L_3 = 2$. E_1 and E_2 are unstable, E_3 and E_4 are stable.

clinic connections between $(\sqrt{3}, \sqrt{3})$ and $(-\sqrt{3}, -\sqrt{3})$, as shown in Fig. 9. Therefore, we can consider using the bifurcation control method to reconfigure the structure in a more realistic way with a smaller change of the spring natural length such that L_2 switches from 2 to 1.3.

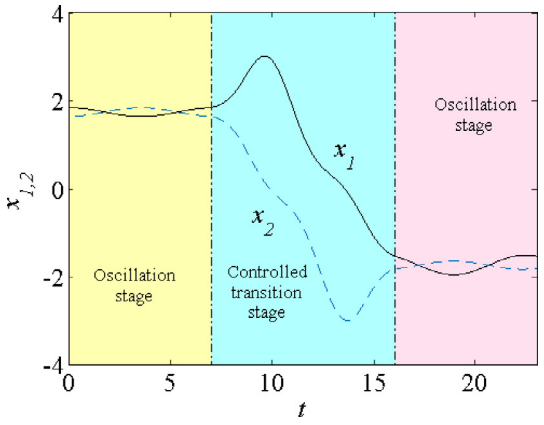

Fig. 8. Controlled transition from E_1 at $(\sqrt{3},\sqrt{3})$ to E_2 at $(-\sqrt{3},-\sqrt{3})$ with bifurcation control. The coupling parameters $L_1 = 2$ and $L_3 = 2$ with L_2 switched from 2.5 to 1 to manipulate the stability properties of E_1 and E_2.

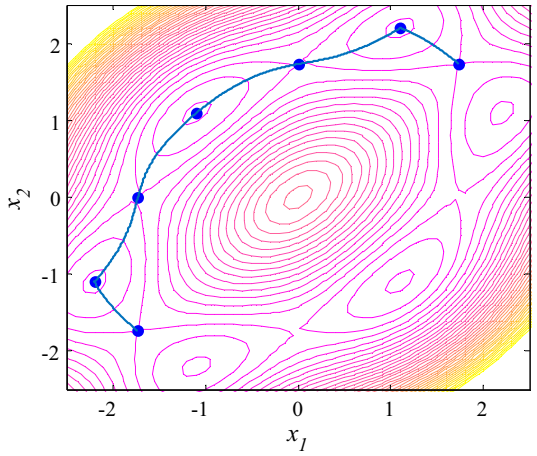

Fig. 9. Potential energy contour plot and ideal path from $(\sqrt{3},\sqrt{3})$ to $(-\sqrt{3},-\sqrt{3})$.

Fig. 10 shows the transition (without dissipation) using this modified bifurcation control. The coupling parameters are $L_1 = 2$ and $L_3 = 2$ with L_2 switched from 2 to 1.3 to manipulate the stability properties of E_1 and E_2. Then, a small displacement is again added to the system in the local minimum potential well to demonstrate capture at the equilibrium point. The initial oscillation of the system in the potential well at E_1 with $L_2 = 1.3$ can therefore be seen, followed by a transition to E_2 with $L_2 = 2$ and then a return to oscillation in the local minimum potential well at E_2 with $L_2 = 1.3$. In addition, the switch process is a simple step change of L_2 from 1.3 to 2, as shown in Fig. 11.

The bifurcation control scheme presented provides the possibility of reconfiguring smart structures using their instability, but retaining stability for normal operating modes. Although the natural length of the spring is varied for illustration, we could also consider additional parameters, such as the spring stiffness k or the spacing d between springs to reduce the variation of the length of the spring. The purpose of the numerical examples presented above is to demonstrate the characteristics and utilisation of bifurcations in this type of nonlinear system. Therefore, an easily visualized means (e.g. natural length of the springs) are used to achieve the reconfiguring process.

4. Controlled heteroclinic connections in a dissipative system

As noted earlier, dissipation needs to be considered for a realistic model where Eq. (4) and (5) show the total energy $W = T + V$ of the system is monotonically decreasing as $\dot{W} = -\beta(p_1^2 + p_2^2)$ corresponding to the general condition $p_1 \neq 0,\ p_2 \neq 0$. In order to proceed it will be assumed that each spring can now be manipulated with variations of the real spring length ΔL by using smart materials such as shape memory polymers, so from Eqs. (7) and (9) it can be seen that

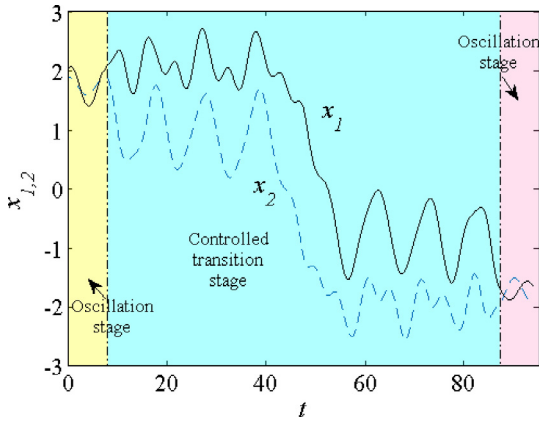

Fig. 10. Controlled transition from E_1 at $(\sqrt{3},\sqrt{3})$ to E_2 at $(-\sqrt{3},-\sqrt{3})$ with bifurcation control with L_2 switched from 1.3 to 2 to manipulate the stability properties of E_1 and E_2.

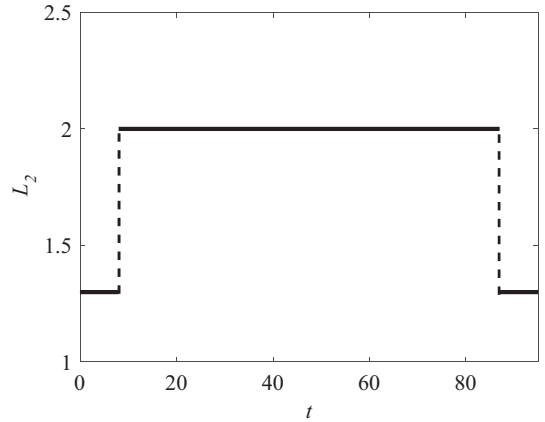

Fig. 11. A step change of L_2 (1.3–2) during the bifurcation control.

$$\dot{p}_1 p_1 - \frac{((L_1+\Delta L_1)-\sqrt{(x_1^2+1)})k_1 x_1}{\sqrt{(x_1^2+1)}}p_1 - \frac{((L_2+\Delta L_2)-\sqrt{((x_1-x_2)^2+1)})k_2(x_1-x_2)}{(\sqrt{(x_1-x_2)^2+1})}p_1 = -\beta p_1^2 \tag{13}$$

$$\dot{p}_2 p_2 - \frac{((L_3+\Delta L_3)-\sqrt{(x_2^2+1)})k_3 x_2}{\sqrt{(x_2^2+1)}}p_2 + \frac{((L_2+\Delta L_2)-\sqrt{((x_1-x_2)^2+1)})k_2(x_1-x_2)}{(\sqrt{(x_1-x_2)^2+1})}p_2 = -\beta p_2^2 \tag{14}$$

which can be written as

$$\frac{d}{dt}(T+V) = -\beta p_1^2 + \frac{\Delta L_1 k_1 x_1}{\sqrt{(x_1^2+1)}}p_1 - \beta p_2^2 + \frac{\Delta L_3 k_3 x_2}{\sqrt{(x_2^2+1)}}p_2 + \frac{\Delta L_2 k_2(x_1-x_2)}{(\sqrt{(x_1-x_2)^2+1})}(p_1-p_2) \tag{15}$$

and is clearly a statement of conservation of power. If It is considered that the system is forced to be conservative then $d(T+V)/dt = 0$, therefore, ΔL can be used to compensate for dissipation by continuous control. Alternatively, a simpler control strategy is to define a controller which can capture the phase space trajectory in the neighbourhood of the target equilibrium point. The difference between the two methods can be seen in Fig. 12. The end-point control strategy provides an easy way to reconfigure smart structures from some initial state to a target state, which uses the controller to compensate the offset caused by dissipation in a planned control region, as shown in Fig. 12a. Conversely, the continuous strategy can be controlled by constantly monitoring and controlling states during the reconfiguration of the smart structure, as shown in Fig. 12b.

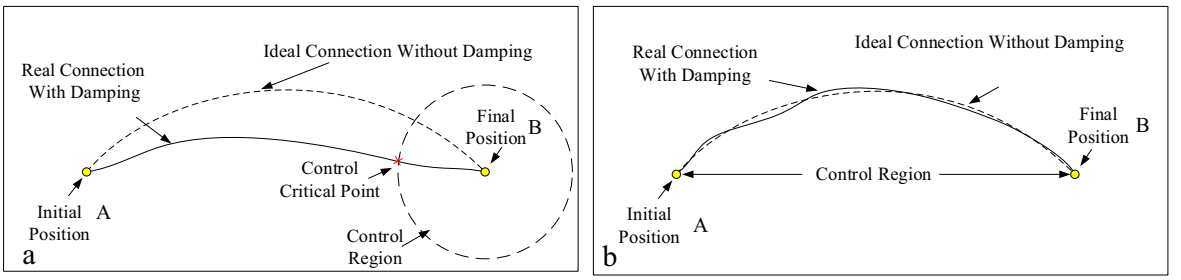

Fig. 12. Control strategy (a) end-point control and (b) continuous control.

4.1. End-point control

In order to ensure convergence to some equilibrium point $(\tilde{x}_1, \tilde{x}_2)$ a Lyapunov function is defined such that

$$\phi(\boldsymbol{x}, \boldsymbol{L}) = \frac{1}{2}p_1^2 + \frac{1}{2}p_2^2 + \frac{1}{2}(x_1 - \tilde{x}_1)^2 + \frac{1}{2}(x_2 - \tilde{x}_2)^2 \tag{16}$$

where $\phi(\boldsymbol{x}, \boldsymbol{L}) > 0$ and $\phi(\tilde{x}_1, \tilde{x}_2) = 0$. The time derivative of the Lyapunov function is clearly

$$\dot{\phi}(\boldsymbol{x}, \boldsymbol{L}) = p_1(\dot{p}_1 + (x_1 - \tilde{x}_1)) + p_2(\dot{p}_2 + (x_2 - \tilde{x}_2)) \tag{17}$$

Then, substituting from the Eq. (7) and (9) the controller for L_1, L_2 and L_3 can be defined as

$$L_1 = -\frac{\sqrt{(x_1^2 + 1)}}{k_1 x_1}\left(\eta p_1 + (x_1 - \tilde{x}_1) - \frac{(L_2 - \sqrt{((x_1 - x_2)^2 + 1)})k_2(x_1 - x_2)}{(\sqrt{(x_1 - x_2)^2 + 1})} - k_1 x_1\right) \tag{18}$$

$$L_2 = -\frac{\sqrt{(x_1 - x_2)^2 + 1}}{k_2(x_1 - x_2)}\left(\eta p_1 + (x_1 - \tilde{x}_1) + \frac{(L_1 - \sqrt{(x_1^2 + 1)})k_1 x_1}{\sqrt{(x_1^2 + 1)}} - k_2(x_1 - x_2)\right) \tag{19}$$

$$L_3 = -\frac{\sqrt{(x_2^2 + 1)}}{k_3 x_2}\left(\eta p_2 + (x_2 - \tilde{x}_2) - \frac{(L_2 - \sqrt{((x_1 - x_2)^2 + 1)})k_2(x_1 - x_2)}{(\sqrt{(x_1 - x_2)^2 + 1})} - k_3 x_2\right) \tag{20}$$

for some control parameter η. It is noted that the system has 2 state variables x_1 and x_2, which can select two controllers from L_1, L_2 and L_3 as control variables to avoid singularities. For example, since $k_2(x_1 - x_2) \neq 0$, $k_3 x_2 \neq 0$ in the neighbourhood of the required equilibrium point E_{10}, L_2 and L_3 are selected as controllers in the neighbourhood of that point.

It can then be seen that ϕ is monotonically decreasing such that

$$\dot{\phi}(\boldsymbol{x}, \boldsymbol{L}) = -(\eta + \beta)(p_1^2 + p_2^2) \leqslant 0 \tag{21}$$

and so $\boldsymbol{x} \to (\tilde{x}_1, \tilde{x}_2)$ and $\boldsymbol{p} \to (0, 0)$ within the neighbourhood of target point.

An example of controlled heteroclinic connections for $\beta = 0.01$ and $\beta = 0.05$ are shown in Fig. 13 for a reconfiguration between E_9 and E_{10}. To initiate the heteroclinic connection, a displacement along the unstable manifold of E_9 is preformed and the controller will be activated when the phase space path is in the defined neighbourhood R of E_{10} ($\eta = 3$). The corresponding controls L_2 and L_3 are shown in Fig. 14. It can be seen that the controls are only active when the phase space path is in the end-point region of E_{10}. Numerical results demonstrate that the control effort grows with increasing dissipation parameter β. That is, the control region needs to be enlarged to fit the increasing dissipation parameter β as shown in Fig. 13.

4.2. Continuous control

For comparison with the end-point control strategy, a continuous control method is now investigated to approximate the heteroclinic connection. This problem is revisited as a computational optimal control problem to determine the control histories which meet the boundary conditions of the problem. In addition to satisfying the state boundary conditions, these control histories also need to minimise a performance index function. Then, the optimal tool PSOPT is employed to solve this optimal control problem numerically using the direct method. PSOPT is coded in C++ by Becerra [26] and is free and open source. The code can deal with many numerical optimisation problems, in particular with endpoint constraints, path constraints, and interior point constraints. Moreover, it can solve the non-linear programming (NLP) problem by using IPOPT, which is an interior point method for large-scale problems.

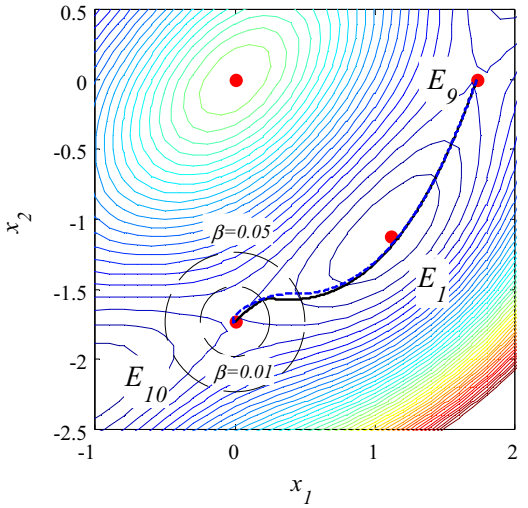

Fig. 13. Controlled transition from E_9 at (1.732051,0) to E_{10} at (0,−1.73205) with the controller active in the neighbourhood of E_{10} with different dissipation. Solid line: dissipation parameter $\beta = 0.01$, dashed line: dissipation parameter $\beta = 0.05$.

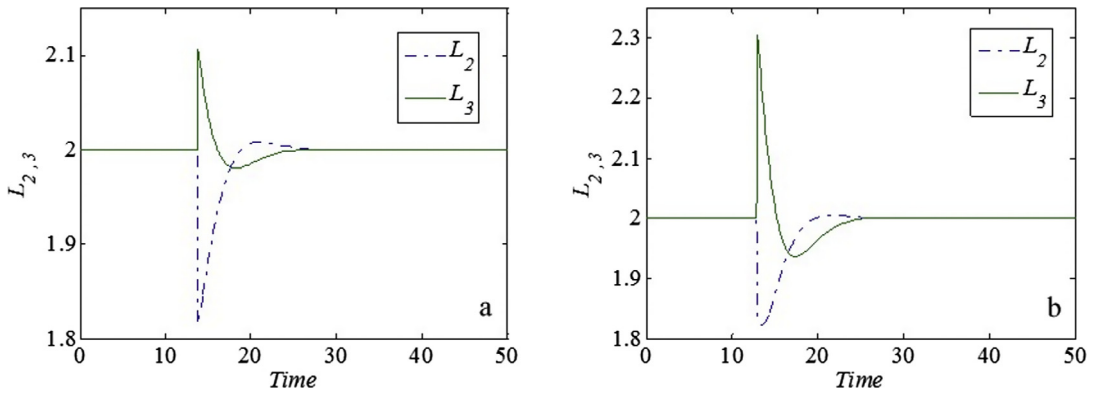

Fig. 14. Controlled transition from E_9 at (1.732051,0) to E_{10} at (0,−1.73205) with the controls actuated through L_2 and L_3 in the neighbourhood of E_{10}. (a) Dissipation parameter $\beta = 0.01$. (b) Dissipation parameter $\beta = 0.05$.

The system can be considered under quasi-static conditions, so that the energy required for each controller can be defined as

$$E = \frac{1}{2}k(\Delta L)^2 \tag{22}$$

where k is the spring stiffness and ΔL is variation of the spring natural length. Therefore, the performance index of the system can be defined

$$J = \int_0^{t_f} ((\Delta L_1)^2 + (\Delta L_2)^2 + (\Delta L_3)^2)dt \tag{23}$$

where t_f means the duration from initial condition to the final condition, then, we define conditions for a transition from the unstable equilibrium E_9 to E_{10} as

$$[\boldsymbol{x}(0) \quad \boldsymbol{x}(T) \quad \dot{\boldsymbol{x}}(0) \quad \dot{\boldsymbol{x}}(T)\,] = \begin{bmatrix} 1.732 & 0 & 0 & 0 \\ 0 & -1.732 & 0 & 0 \end{bmatrix} \tag{24}$$

The numerical results for dissipation parameters $\beta = 0.01$ and $\beta = 0.05$ are shown in Fig. 15. The corresponding controls L_1, L_2 and L_3 are shown in Fig. 16. It can be seen that the controls are symmetric about the point $t = T/2$ as expected. Moreover, in general more energy is required to compensate for a larger dissipation parameter β, which means the range of the controller becomes larger for the reconfiguration, as shown in Fig 16.

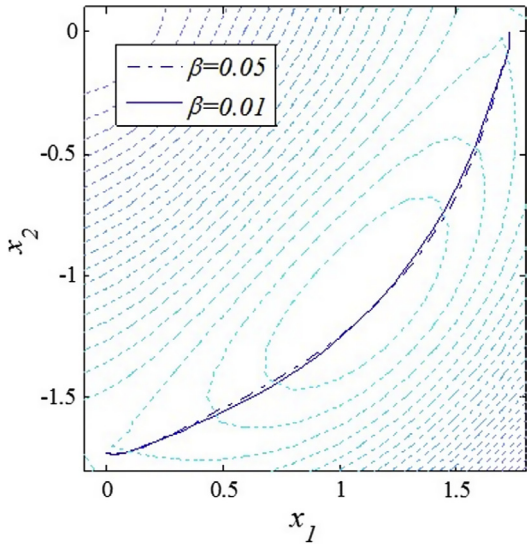

Fig. 15. Controlled transition from E_9 at $(1.732051, 0)$ to E_{10} at $(0, -1.73205)$ with the controller active under the continuous control method (dissipation parameters $\beta = 0.01, 0.05$).

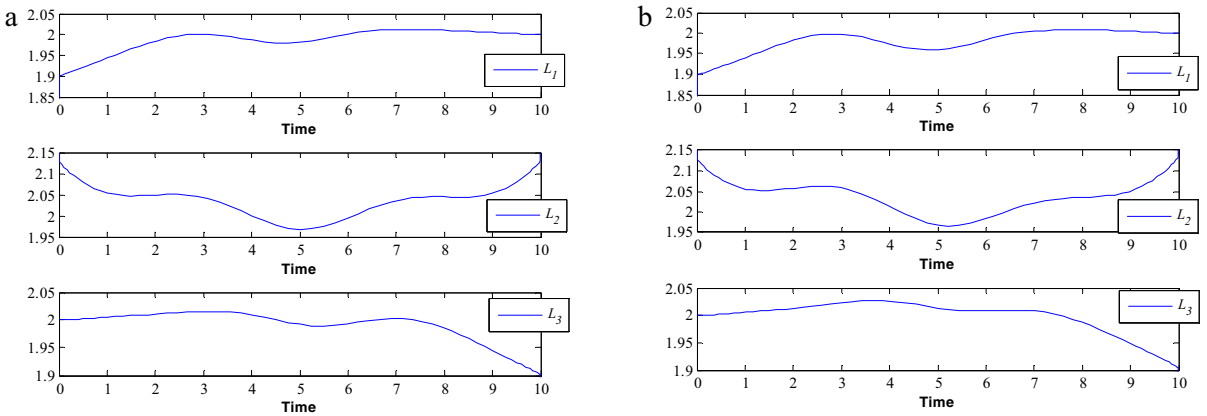

Fig. 16. Controlled transition from E_9 at $(1.732051, 0)$ to E_{10} at $(0, -1.73205)$ with the controls actuated through L_1, L_2 and L_3 under the continuous control method. (a) Dissipation parameters $\beta = 0.01$. (b) Dissipation parameter $\beta = 0.05$.

In order to keep the structure model simple, some assumptions and simplifications were proposed to implement the research, for example, the dissipation was assumed as linear relationship. The model used in this paper has some differences with a real structural model, omitting material viscosity, time lag effects of the control. Through using this qualitatively simple model, new insights can be obtained on the use of heteroclinic connections. This simple model can be used to introduce this new reconfiguration concept and provide insights for use in a more accurate high fidelity model [27]. Although the end-point control method is easy, it needs an instantaneous control in the reconfiguration procedure. Besides, most importantly, it may be difficult to find exact heteroclinic connections numerically in complex nonlinear dynamic systems. In contrast, the continuous control method could provide a more smooth controlled transitions with less energy, but it may be computationally intensive to determine. Therefore, a smart structure can be reconfigured from one unstable state to another through choosing a suitable control maneuver from the end-point control and the continuous control method. In addition, the utilisation of these two methods can be clarified for different systems, for example, the end-point method could be adequate for lightly damped systems and the continuous control methods can provide satisfactory state trajectories with small changes in control variables.

Moreover, a better reconfigurable strategy is used to combine bifurcation control and controlled heteroclinic connections, which is expected to reconfigure real smart structures between stable states. For example, structures are assumed initially in local stable states. Through performing bifurcation the local condition becomes unstable. Then, bifurcation is performed again when end-point control generates a trajectory to the target equilibrium point. This represents a computationally efficient way to achieve reconfiguration for smart structures between two different equilibria positions with less energy.

5. Conclusion

A multi-stable smart structure has been modelled using a simple, representative spring mass chain. In general, such a system has a set of stable states separated by unstable, some with equal energy. Therefore, smart structures can in principle be reconfigured by using their instability. After changing the characteristics of the system by using bifurcation theory, these unstable configurations will be used to develop energy-efficient schemes to reconfigure the smart structure. In principle, such reconfigurations do not require the input of energy, other than to overcome dissipation in the system. Then, two ways to reconfigure smart structures have been presented to compensate for damping in the reconfiguring. It was found that the transition between unstable equilibria can be achieved through manipulation of the natural length of the springs in the model with linear dissipation, which is assumed to be achieved with a suitable active material. While the model used is simple, it provides insights into the problem which can be exploited to develop the concept towards the reconfiguration of real smart structures.

Acknowledgments

McInnes was support by a Leverhulme Trust Fellowship and a Royal Society Wolfson Research Merit Award.

References

[1] L.L. Howell, S.P. Magleby, B.M. Olsen, Handbook of Compliant Mechanisms, John Wiley & Sons, 2013.
[2] A. Brinkmeyer, A. Pirrera, M. Santer, P.M. Weaver, Pseudo-bistable pre-stressed morphing composite panels, Int. J. Solids Struct. 50 (2013) 1033–1043.
[3] S. Daynes, A. Grisdale, A. Seddon, R. Trask, Morphing structures using soft polymers for active deployment, Smart Mater. Struct. 23 (2014) 012001.
[4] O. Guenther, T. Hogg, B.A. Huberman, Controls for unstable structures Smart Structures and Materials 1997: mathematics and control in smart structures, in: The Society of Photo-Optical Instrumentation Engineers (SPIE) Conf. (June), Proc. SPIE, 1997, pp. 754–763.
[5] D.-Y. Lee, J. Kim, J.-S. Kim, C. Baek, G. Noh, D.-N. Kim, K. Kim, S. Kang, K.-J. Cho, Anisotropic patterning to reduce instability of concentric-tube robots, IEEE Trans. Robot. 31 (2015) 1311–1323.
[6] T. Hogg, B.A. Huberman, Controlling smart matter, Smart Mater. Struct. 7 (1998) R1–R14.
[7] J. Terrence, F. Mary, G. Farhan, A bistable mechanism for chord extension morphing rotors, in: SPIE Smart Structures and Materials Nondestructive Evaluation and Health Monitoring (International Society for Optics and Photonics), 2009, pp. 72881C1-12.
[8] K.-J. Lu, S. Kota, Design of compliant mechanisms for morphing structural shapes, J. Intell. Mater. Syst. Struct. 14 (2003) 379–391.
[9] B. Camescasse, A. Fernandes, J. Pouget, Bistable buckled beam: elastica modeling and analysis of static actuation, Int. J. Solids Struct. 50 (2013) 2881–2893.
[10] B. Camescasse, A. Fernandes, J. Pouget, Bistable buckled beam and force actuation: experimental validations, Int. J. Solids Struct. 51 (2014) 1750–1757.
[11] D.C. Lagoudas, Shape Memory Alloys: Modeling and Engineering Applications, Springer, New York, 2008.
[12] A.B. Flatau, K.P. Chong, Dynamic smart material and structural systems, Eng. Struct. 24 (2002) 261–270.
[13] J. Mohd Jani, M. Leary, A. Subic, M.a. Gibson, A review of shape memory alloy research, applications and opportunities, Mater. Des. 56 (2014) 1078–1113.
[14] M. Behl, K. Kratz, J. Zotzmann, U. Nöchel, A. Lendlein, Reversible bidirectional shape-memory polymers, Adv. Mater. 25 (2013) 4466–4469.
[15] M. Behl, K. Kratz, U. Noechel, T. Sauter, A. Lendlein, Temperature-memory polymer actuators, Proc. Natl. Acad. Sci. U.S.A. 110 (2013) 12555–12559.
[16] S. Hurlebaus, L. Gaul, Smart structure dynamics, Mech. Syst. Signal Process. 20 (2006) 255–281.
[17] M.T. Tolley, S.M. Felton, S. Miyashita, D. Aukes, D. Rus, R.J. Wood, Self-folding origami: shape memory composites activated by uniform heating, Smart Mater. Struct. 23 (2014) 094006.
[18] S. Felton, M. Tolley, E. Demaine, D. Rus, R. Wood, A method for building self-folding machines, Science (80-.) 345 (2014) 644–646.
[19] E. Hawkes, B. An, N.M. Benbernou, H. Tanaka, S. Kim, E.D. Demaine, D. Rus, R.J. Wood, Programmable matter by folding, Proc. Natl. Acad. Sci. U.S.A. 107 (2010) 12441–12445.
[20] C.R. McInnes, T.J. Waters, Reconfiguring smart structures using phase space connections, Smart Mater. Struct. 17 (2008) 025030.
[21] C.R. McInnes, D.G. Gorman, M.P. Cartmell, Enhanced vibrational energy harvesting using nonlinear stochastic resonance, J. Sound Vib. 318 (2008) 655–662.
[22] J. Zhang, C.R. McInnes, Reconfiguring smart structures using approximate heteroclinic connections, Smart Mater. Struct. 24 (2015) 105034.
[23] J. Zhang, C.R. McInnes, Reconfiguring smart structures using approximate heteroclinic connections in a spring-mass model, in: Proceedings of the ASME Conference on Smart Materials, Adaptive Structures and Intelligent Systems (SMASIS 2015) (Colorado Springs), 2015.
[24] S. Wiggins, Introduction to Applied Nonlinear Dynamical Systems and Chaos, Springer, New York, 1990.
[25] Y.S. Oh, S. Kota, Synthesis of multistable equilibrium compliant mechanisms using combinations of bistable mechanisms, J. Mech. Des. 131 (2009) 021002.
[26] V.M. Becerra, Solving complex optimal control problems at no cost with PSOPT, in: 2010 IEEE Int. Symp. Comput. Control Syst. Des., 2010, pp. 1391–1396.
[27] S.S. Ganji, A. Barari, D.D. Ganji, et al, Approximate analysis of two-mass-spring systems and buckling of a column, Comput. Math. Appl. 61 (4) (2011).